



ESA Climate Change Initiative – Fire_cci

D2.2.2 Algorithm Theoretical Basis Document (ATBD) – Small Fires Dataset – Long Term Pilot Sites (SFDL)

Project Name	ECV Fire Disturbance: Fire_cci
Contract N°	4000126706/19/I-NB
Issue Date	18/12/2023
Version	1.2
Author	Amin Khairoun, Erika Solano
Document Ref.	Fire_cci_D2.1.4_ATBD_SFDL_v1.2
Document type	Public

To be cited as: Khairoun, A., Solano, E. (2023) ESA CCI ECV Fire Disturbance: D2.2.2 Algorithm Theoretical Basis Document-SFDL, version 1.2. Available at: <https://climate.esa.int/en/projects/fire/key-documents/>

	Fire_cci	Ref.:	Fire_cci_D2.2.2_ATBD_SFDL_v1.2		
	Algorithm Theoretical Basis Document Small Fires Dataset Long Term	Issue	1.2	Date	18/12/2023
		Page	2		

Prime Contractor/ Scientific Lead & Project Management	UAH – University of Alcalá (Spain)
Earth Observation Team	UAH – University of Alcalá (Spain) UPM – Universidad Politécnica de Madrid (Spain) CNR-IREA - National Research Council of Italy – Institute for Electromagnetic Sensing of the Environment (Italy)
System Engineering	BC – Brockmann Consult (Germany)
Climate Modelling Group	CNRS - Laboratory for Sciences of Climate and Environment (France) VU - Vrije Universiteit Amsterdam (Netherlands)



Distribution

Affiliation	Name	Address	Copies
ESA	Clément Albergel (ESA)	clement.albergel@esa.int	electronic copy
Project Team	Emilio Chuvieco (UAH)	emilio.chuvieco@uah.es	electronic copy
	M. Lucrecia Pettinari (UAH)	mlucaresia.pettinari@uah.es	
	Amin Khairoun (UAH)	amin.khairoun@uah.es	
	Erika Solano (UAH)	erika.solano@uah.es	
	Consuelo Gonzalo (UPM)	consuelo.gonzalo@upm.es	
	Dionisio Rodríguez (UPM)	dionisio.rodriguez@ulpgc.es	
	Ángel García Pedrero (UPM)	angelmario.garcia@upm.es	
	Daniela Stroppiana (CNR)	stroppiana.d@irea.cnr.it	
	Thomas Storm (BC)	thomas.storm@brockmann-consult.de	
	Martin Böttcher (BC)	martin.boettcher@ brockmann-consult.de	
	Florent Mouillot (CNRS)	florent.mouillot@cefe.cnrs.fr	
	Philippe Ciaï (CNRS)	philippe.ciaï@lsce.ipsl.fr	
	Guido van der Werf (VUA)	g.r.vander.werf@vu.nl	

	<p style="text-align: center;">Fire_cci Algorithm Theoretical Basis Document Small Fires Dataset Long Term</p>	Ref.:	Fire_cci_D2.2.2_ATBD_SFDL_v1.2			
		Issue	1.2	Date	18/12/2023	
		Page				3

Summary

This document describes the algorithm used for generating a long term Small Fire Dataset (SFDL) in three pilot sites across the world with data from the Landsat satellites covering from 1990 to 2019.

	Affiliation/Function	Name	Date
Prepared	UAH	Amin Khairoun Erika Solano	14/12/2023
Reviewed	UAH – Project Manager	Lucrecia Pettinari	14/12/2023
Authorized	UAH - Science Leader	Emilio Chuvieco	14/12/2023
Accepted	ESA - Technical Officer	Clément Albergel	

This document is not signed. It is provided as an electronic copy.

Document Status Sheet

Issue	Date	Details
1.0	30/11/2023	First public release of the document
1.1	14/12/2023	Addressing comments from ESA's Technical Officer

Document Change Record

Issue	Date	Request	Location	Details
1.1	14/12/2023	ESA	Sections 2, 3.1, 3.2.1, 3.3.4	Small changes in the text
1.2	18/12/2023	ESA	Section 2	Additional clarification on the use of Sentinel-2 data.

	<p style="text-align: center;">Fire_cci Algorithm Theoretical Basis Document Small Fires Dataset Long Term</p>	Ref.:	Fire_cci_D2.2.2_ATBD_SFDL_v1.2		
		Issue	1.2	Date	18/12/2023
		Page			4

Table of Contents

1	Executive Summary	6
2	Introduction.....	6
3	Data and Methods	8
3.1	Pilot sites location	8
3.2	Input datasets and pre-processing	10
3.2.1	Landsat surface reflectance	10
3.2.2	Ancillary Datasets.....	11
3.3	Burned area processing	12
3.3.1	General overview of the algorithm	12
3.3.2	Selection of processing periods	14
3.3.3	Spectral indices.....	15
3.3.4	Multitemporal compositing	16
3.3.5	Additional masking	16
3.3.6	Random Forest Classifier	17
3.3.7	Generation of preliminary burned area.....	18
3.3.8	Impact of the use of mosaicking date as predictor	18
3.3.9	Generation of final burned area	19
3.3.10	Enhancement of fire detection dates in Siberia	21
4	Layer output results.....	22
5	Limitations of the product.....	23
6	References	24
	Annex: Acronyms and abbreviations	27

	<p style="text-align: center;">Fire_cci Algorithm Theoretical Basis Document Small Fires Dataset Long Term</p>	Ref.:	Fire_cci_D2.2.2_ATBD_SFDL_v1.2		
		Issue	1.2	Date	18/12/2023
		Page	5		

List of Figures

Figure 1. Location of the 3 regions covered by the long-term high-resolution BA record (30 years).	10
Figure 2. Flowchart of the general overview of FireCCISFDL10 BA product.....	13
Figure 3. Fire seasonality across pilot sites using FireCCI51 time series.	14
Figure 4. Number of periods proposed in each zone in function of image availability: A) Sahel; B) Amazonia; C) Siberia.	15
Figure 5. Mitigation of Landsat 5 defective values in 2001-2002: A) and B) are False colour composites using NBR2-NIR-Red band combination before and after applying the filter, respectively. C) and D) show the RF classification probability on top of false colour composites before and after applying the filter, respectively...	17
Figure 6. Burned area delineation process for some fire events in the northern border between Paraguay and Argentina for the period 2016-04-01 to 2016-09-30: A) Pre-composite (from 2015-10-01 to 2016-03-31); B) Post-composite (from 2016-04-01 to 2016-09-30); C) The difference composite; D) RF classification probability; E) Seeds; F) Delineation of preliminary BA patches. All False colour composites use NBR2-NIR-Red band combination.	18
Figure 7. Impact of the use of date difference between composites in the predicted BA probability in western Siberia in 2019: A) Pre-time series false colour composite; B) Post-time series false colour composite; C) BA classification without date difference as predictor; D) BA classification including the date difference as predictor. All False colour composites use NBR2-NIR-Red band combination.	19
Figure 8. Generation of the final BA patches: A) Post-time series false colour composite; B) Classification probabilities of preliminary BA; C) Classification probabilities after relaxed growing region; D) Final BA patch after applying geomorphological operations.	21
Figure 9. Correction of burn detection dates in Siberia fires using active fires: A) JD layer before date correction; B) Active fires detected within the BA patch; C) Result of the JD correction.....	22
Figure 10. FireCCISFDL10 output layers' example of tile 16S060W in Amazonia for months April to September 2019 (all months combined): A) Post-time series false colour composite; B) Julian day; C) Probability; D) Land cover.....	23

List of Tables

Table 1. Selected bands for every Landsat satellite and sensor, and their approximate wavelengths.	11
Table 2. Bit Values and conditions applied for masking of Landsat data.	11
Table 3. Burnable land cover types in HRLC CCI maps	12
Table 4. Contents of FireCCISFDL10 layers	22

	<p style="text-align: center;">Fire_cci Algorithm Theoretical Basis Document Small Fires Dataset Long Term</p>	Ref.:	Fire_cci_D2.2.2_ATBD_SFDL_v1.2			
		Issue	1.2	Date	18/12/2023	
		Page				6

1 Executive Summary

Fires emit greenhouse gases and aerosols, important climate forcing factors, which need to be estimated and modelled to understand better climate and carbon cycling. Fires are also a major factor in land cover change, and hence affect fluxes of energy and water to the atmosphere. In this context, spatial and temporal monitoring of trace gas emissions from fires is of primary importance. These can be inferred using both land-surface and atmospheric measurements, preferably in combination. The Fire Disturbance Essential Climate Variable provides baseline products for the land-surface to allow this.

Burned area (BA), as derived from satellites, is considered the primary variable that requires climate-standard continuity. It can be combined with information on burn efficiency and available fuel load to estimate emissions of trace gases and aerosols. Measurements of BA may be used as direct input (driver) to climate and carbon cycle models or, when long time series of data are available, to parameterise climate-driven models for BA (GCOS, 2022).

This document is the Algorithm Theoretical Basis Document (ATBD) corresponding to the generation of the long-term Small Fire Datasets for pilot sites in Amazonia, Sahel and Siberia extending from 1990 to 2019 at high-resolution (~30 m at the equator). The theoretical basis described here identifies the data sets that were used to classify burned area and the describes the methodology employed to derive the BA products.

2 Introduction

Common global BA products are based on coarse and medium resolution sensors (from 250 to 1000 m). Therefore, the likelihood of detecting small burns (i.e., < 50 ha) is very low, and for this reason omission errors from these products may be quite high (Boschetti et al. 2019, Franquesa et al. 2022) particularly coming from small fires (Randerson et al. 2012). In order to improve the characterisation of small fires, one of the objectives of the project is to generate a small fires datasets (SFD) based on high-resolution sensors (10 to 30 m). Considering the enormous processing effort to cover the entire planet, this SFD dataset focuses on three areas of interest. The first SFD product generated, named FireCCISFD11, was produced within the Phase 2 of the FireCCI project and contained areas burned in 2016 in Sub-Saharan Africa (Roteta et al. 2019), while the second SFD, called FireCCISFD20, was generated in the same region but for 2019 (Chuvieco et al. 2022). Both versions were based on Sentinel-2 data. In the current version of the SFD, we aim to focus more on the regions in-line with the High Resolution Land Cover (HRLC) CCI project and therefore the covered areas are parts of Amazonia, Africa and Siberia, for which long-term BA archives covering 30 years (1990-2019) based on Landsat imagery at 30 m were processed.

Since coarse-resolution burned area detection algorithms require that a substantial fraction of an individual pixel's area is burned for successful attribution (to avoid commission errors from other forms of land cover change), detection of small fires becomes difficult (Roy and Landmann, 2005). At a global scale, it has been shown that

	<p style="text-align: center;">Fire_cci Algorithm Theoretical Basis Document Small Fires Dataset Long Term</p>	Ref.:	Fire_cci_D2.2.2_ATBD_SFDL_v1.2			
		Issue	1.2	Date	18/12/2023	
		Page				7

accounting for small fires may increase burned area and global carbon emissions by approximately 35% (Randerson et al., 2012). At continental scale, the use of high-resolution BA (for example FireCCISFD20 derived from Sentinel-2A and B) proved that omission (OE) and commission errors (CE) could be reduced to 8.5 and 15.0 %, respectively in comparison with medium resolution BA products such as FireCCI51 (OE = 49.3 % and CE = 24.9 %) and MCD64A1 (OE = 54.1% and CE = 20.9%) derived from MODIS (Chuvieco et al., 2022; Stroppiana et al., 2022). This improvement of accuracy especially in terms of omission errors led to significantly higher BA estimations (80% greater than FireCCI51 and 120 % larger than MCD64A1) over sub-Saharan Africa in 2019. The first version of the SFD (FireCCISFD11), which was generated using a single Sentinel-2 satellite, estimated twice more fire emissions than MCD64A1 in 2016 over the same area and the underestimation of fire impacts using coarse-resolution BA products was mainly attributed to their high omission of small fires (Ramo et al., 2021).

The capability of Landsat imagery to provide information on burned patches has been widely recognized in scientific literature due to its long temporal coverage (1984 onwards), its high spatial resolution (30 m) and multispectral characteristics (covering the most important spectral areas for burned area mapping with one band in the near infrared and two in the shortwave infrared). Subsequently, several studies used Landsat data to derive BA at local to regional scale (Bastarrika et al., 2014; Bastarrika et al., 2011; Boschetti et al., 2015; Chuvieco et al., 2002). Recent developments aimed to use the capabilities of the Google Earth Engine (GEE) cloud computing platform to generate long-term large scale burned area archives at national (Alencar et al., 2022) and large regional scales (Descals et al., 2022) and concluded that this platform provides a high potential of assessment of BA trends at these scales once it is used efficiently. Currently, the only global BA product using high-resolution data is called GABAM (Long et al. 2019), extending over the entire time series of Landsat until 2021. Yet, this product manifests several discrepancies. In fact, it shows a large amount of omissions (Roteta et al. 2021b) even higher than coarse-resolution BA products, which explains the reason why it detects less than 4 Mkm² of BA yearly (Wei et al., 2021), lower than the estimations of the two previous versions of SFD in Africa alone (≥ 4.8 Mkm²). Additionally, this global product indicates solely the year of the fire, with no attribution of the burning date.

The aim of this version of the SFD (FireCCISFDL10 in the rest of the document) is to develop a consistent time series database of areas burned in small fires in the three regions above mentioned. For doing that, we rely primarily on Landsat data, as it is the longest time series sensor currently available. Since the time series of FireCCISFDL10 starts in 1990, it was not possible to apply the same methods used in our FireCCISFD20 product, as this latter dataset relies on active fires and these products were either not available or highly uncertain before the MODIS era (pre-2000). For this reason, we have adapted the Burned Area Mapping Tools (BAMT) developed by Roteta et al. (2021a) in GEE. We have enhanced its performance and optimised the different components of the algorithm

	Fire_cci	Ref.:	Fire_cci_D2.2.2_ATBD_SFDL_v1.2		
	Algorithm Theoretical Basis Document Small Fires Dataset Long Term	Issue	1.2	Date	18/12/2023
		Page	8		

in order to develop a long-term archive of BA based on the Landsat imagery archive in three large-scale pilot sites, namely Amazonia, eastern Sahel and Siberia.

We were studying different options to include Sentinel-2 data in the time series, but all of them were unsatisfactory to obtain a consistent output. As consistency is the critical element of this activity, we have finally decided to generate a separate dataset with Sentinel-2 data for the most recent years, for intercomparison purposes. We will rely for this activity on the algorithm developed by Roteta et al. and described in the FireCCISFD20 description paper.

3 Data and Methods

3.1 Pilot sites location

The selection of pilot sites for the generation of long-term BA SFD dataset was based on those selected for the ESA HRLC CCI project, following the recommendations of its Climate User Group, which determined three large pilot areas (see Figure 1) of particular interest to study the climate/land cover feedbacks. These areas cover 3 different continents, climate (tropical, semi-arid, boreal) and present complex surface atmosphere interactions that have significant impacts not only on the regional climate but also on large-scale climate structures. Limited large-scale information about these ecosystems is available at high-resolution to provide an accurate assessment of surface-atmosphere interactions. For this reason, the understanding of their associated vegetation-atmosphere feedbacks are still poorly captured by state-of-the art earth system models, which engender major uncertainties in the research studies aiming to track their history and/or predict their future evolution. Additionally, these regions are critical for the global carbon cycle through the uptake of carbon by terrestrial ecosystems as they encompass major biomes that are vulnerable in terms of land carbon stocks (tropical forest, permafrost) (ESA, 2020a) and desertification processes along with their unfolding resources' sustainability challenges.

The processing regions were limited to the extent in which dynamic HRLC maps are generated within the HRLC CCI project. The three key study areas are described below (ESA, 2020b):

Amazonia: (24°S - 12°S; 47°W - 62°W)

The first region involves the Amazon basin, which has for several decades focused the attention of the scientific community due to large deforestation rates and potential associated large-scale climate impacts. This region extends over a variety of ecosystems including tropical and subtropical savannas (Cerrado) and broadleaf forests, as well as the world's largest tropical wetland (Pantatal). Agricultural expansion and climate variability have become important agents of disturbance in the Amazon basin, mainly in the southern and eastern portions. Although Amazonian forests have considerable resilience to moderate annual drought, the interactions between deforestation, fire and drought potentially lead to losses of carbon storage and changes in regional precipitation

	Fire_cci	Ref.:	Fire_cci_D2.2.2_ATBD_SFDL_v1.2		
	Algorithm Theoretical Basis Document Small Fires Dataset Long Term	Issue	1.2	Date	18/12/2023
		Page	9		

patterns and river discharge with some signs of a transition to a disturbance-dominated regime.

Sahel: (4°N - 16°N; 27°E - 43.5°E)

The second area of interest is the eastern part of the Sahel band in Africa covering more or less the Horn of Africa region. This region is dominated by arid and semi-arid ecoregions such as tropical, subtropical and montane savannas. Additionally, it includes Africa's largest tropical wetland (Sudd grasslands). Eastern Sahel represent one of the most vulnerable regions to climate-related risks characterised by highly variable and irregular rainfall together with rising temperatures, which results in more disastrous and frequent drought and flood events in recent years. However, the impact of El Niño-Southern Oscillation cycle (ENSO) in the initiation of dramatic drought events in this region is still inadequately understood due to the lack of studies compared with Western Sahel, and therefore deserves more study to enhance the predictions of future changes and their consequences on regional climate and on the sustainable development of the population, particularly in terms of food and water security.

Siberia: (60°N - 74°N; 65°E - 86°E)

The third region is located in the northern high latitudes, for which future climate changes are expected to be particularly strong, a phenomenon known as polar amplification, which was clearly affecting the fire regime and its consequences (Descals et al., 2022; Zheng et al., 2023). In Siberia, complex climate feedbacks over land, implicating natural and human factors, may further amplify these changes and make this region a possible hot spot of future climate changes. Siberia represents 10% of the land surface, 30% of forested surfaces globally, and hosts the largest peatland basin worldwide. The warmer temperatures (Hantemirov et al., 2022) and increased winter rainfall have promoted increases in biosphere activity and longer active seasons. Land cover (LC) changes have been reported with the displacement of the forest-shrubs-grasslands transition zone to the north. In addition, changes in LC may impact directly the fate of the carbon stored in permafrost, which in turn will affect long-term terrestrial carbon balance and ultimately climate change, especially under the alarming increase of early snowmelt together with an anomalous Arctic front jet observed during the recent years (Scholten et al., 2022).

	<p style="text-align: center;">Fire_cci Algorithm Theoretical Basis Document Small Fires Dataset Long Term</p>	Ref.:	Fire_cci_D2.2.2_ATBD_SFDL_v1.2		
		Issue	1.2	Date	18/12/2023
		Page	10		

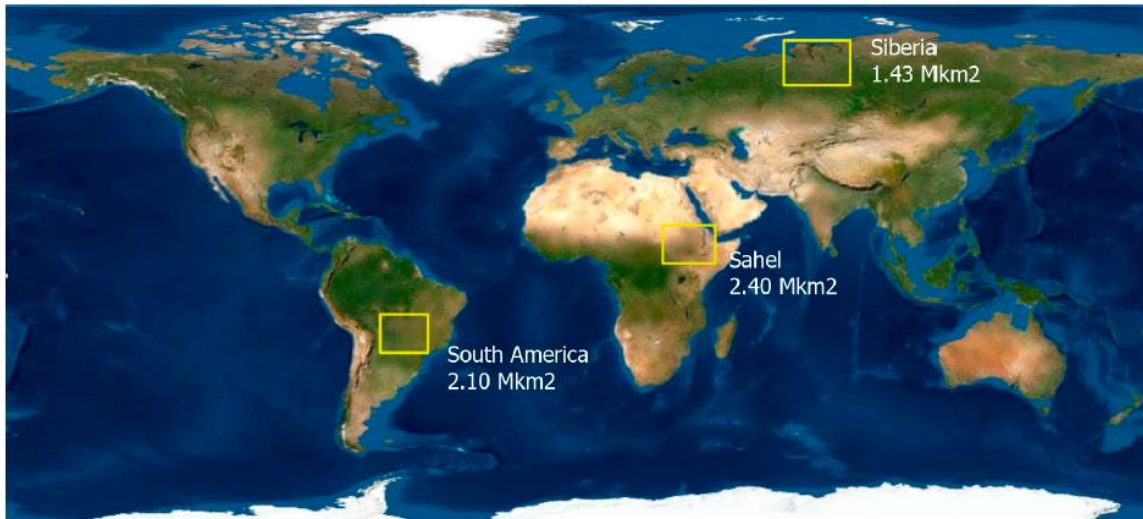


Figure 1. Location of the 3 regions covered by the long-term high-resolution BA record (30 years).

3.2 Input datasets and pre-processing

3.2.1 Landsat surface reflectance

The Landsat program is a NASA/USGS programme for satellite imagery acquisition and Earth observation, with a series of satellites that started acquiring images in 1972 with Landsat-1, being the last satellite launched in late 2021 (Landsat 9), and millions of scenes of the Earth having been acquired since then. From its eight satellites, only Landsat-4 and -5 Thematic Mapper (TM), Landsat-7 Enhanced Thematic Mapper Plus (ETM+) and Landsat-8 Operational Land Imager (OLI) data are used in this SFD. They provide continuous global coverage since 1982, acquiring images every 16 days (reduced to 8 days in years where two satellites are operational) at 30 m of spatial resolution and covering the visible, near infrared (NIR) and short wavelength infrared (SWIR) spectral regions. From all available Landsat products in GEE, the Collection 2 (C2) of Landsat Tier 1 Surface Reflectance (SR) product was the one selected. It includes atmospherically corrected and orthorectified surface reflectance data for four visible and near-infrared and two short wavelength infrared bands. These products are represented by the following IDs in GEE: “LANDSAT/LT04/C02/T1_SR” for Landsat-4 TM, “LANDSAT/LT05/C02/T1_SR” for Landsat-5 TM, “LANDSAT/LE07/C02/T1_SR” for Landsat-7 ETM+ and “LANDSAT/LC08/C02/T1_SR” for Landsat-8 OLI (Roteta et al., 2021a). Surface reflectance of Landsat 4 to 7 is derived using the Landsat Ecosystem Disturbance Adaptive Processing System (LEDAPS) algorithm, while Landsat 8 uses the Land Surface Reflectance Code (LaSRC). Six reflectance bands common to all three sensors (TM, ETM+ and OLI) are employed: the three visible colours (blue, green and red), the NIR and two short wavelength infrareds (short and long SWIRs). Each of these bands’ wavelengths may vary among different sensors, but they cover an equivalent region in the spectrum (Table 1). Landsat bands are available at 30 m spatial resolution.

Table 1. Selected bands for every Landsat satellite and sensor, and their approximate wavelengths.

	Landsat-4 / 5	Landsat-7	Landsat-8 / 9	Approximate Wavelength (μm)
Sensor	TM	ETM+	OLI	-
Blue	B1	B1	B2	0.45-0.52
Green	B2	B2	B3	0.53-0.59
Red	B3	B3	B4	0.63-0.68
NIR	B4	B4	B5	0.80-0.89
Short SWIR	B5	B5	B6	1.55-1.70
Long SWIR	B7	B7	B7	2.10-2.30

3.2.2 Ancillary Datasets

3.2.2.1 Quality assessment band masking

The Quality Assessment (QA) band for Landsat sensors has been used to identify pixels that exhibit adverse instrument, atmospheric or superficial conditions. The PIXEL_QA band is generated using the Function of Mask (FMask) algorithm and presented in a bit-packed form for Landsat images. In our case, pixels showing the presence of clouds, cloud shadows, cirrus or snow were masked out (Table 2).

Table 2. Bit Values and conditions applied for masking of Landsat data.

QA bit	State
2	Cirrus
3	Clouds
4	Cloud shadows
5	Snow

3.2.2.2 Active fire products

Most of BA algorithms rely on active fires to check that the spectral/temporal changes detected in the images are due to fire, where they are used as seeds before applying growing processes. In the case of the FireCCISFDL10 BA algorithm, times series extends beyond the coverage of existing active fire data archives (which starts in November 2000 in the case of MODIS) and the use of other proxies to create seeds was required. BA detection in FireCCISFDL10 is independent of active fires.

Still, they were used to enhance fire detection dates in the case of Siberia where image acquisitions are limited because of frequent cloud coverage. For that purpose, we used the Collection 2 of the VNP14IMGML product derived from the Suomi National Polar-orbiting Partnership Visible Infrared Imaging Radiometer Suite sensor (S-NPP/VIIRS) at 375 m spatial resolution from 2012 onward, whereas the period 2001-2011 was enhanced

	<p style="text-align: center;">Fire_cci Algorithm Theoretical Basis Document Small Fires Dataset Long Term</p>	Ref.:	Fire_cci_D2.2.2_ATBD_SFDL_v1.2			
		Issue	1.2	Date	18/12/2023	
		Page				12

using the Collection 6.1 of MCD14DL hotspots derived from MODIS at 1 km spatial resolution (from Aqua and Terra satellites jointly). Both datasets are downloaded from the NASA FIRMS platform (<https://firms.modaps.eosdis.nasa.gov/download/>, last accessed in October 2023).

3.2.2.3 Land cover information

The FireCCISFDL10 pilot sites were selected to fit the regions for which long-term dynamic land cover maps were generated within the HRLC CCI project. This project provides to the climate community land cover maps at the resolution of 10-30 m of Amazonia, Sahel and western Siberia. The main sources of information include Sentinel-2 and Landsat for optical imagery and Sentinel-1 for radar data (ESA, 2020a). These maps served to mask burnable land cover types and to assign the land cover of each burned pixel. A full description of the different land cover types is shown in Table 3.

Table 3. Burnable land cover types in HRLC CCI maps

Value	LC type description	Burnable
0	No data	
10	Tree cover evergreen broadleaf	x
20	Tree cover evergreen needleleaf	x
30	Tree cover deciduous broadleaf	x
40	Tree cover deciduous needleleaf	x
50	Shrub cover evergreen	x
60	Shrub cover deciduous	x
70	Grasslands	x
80	Croplands	x
90	Woody vegetation aquatic or regularly flooded	x
100	Grassland vegetation aquatic or regularly flooded	x
110	Lichens and mosses	x
120	Bare areas	
130	Built-up	
140	Open water	
141	Open water seasonal	
142	Open water permanent	
150	Permanent snow and/or ice	

3.3 Burned area processing

3.3.1 General overview of the algorithm

The algorithm includes two phases: 1) the main phase of BA classification in Google Earth Engine platform (GEE) and 2) the post-processing and enhancement phase performed locally. The first phase aims to generate a BA vector map as well as its

corresponding ancillary layers (i.e., probability and Julian day of burn) in a user-defined area (each of our pilot sites) and period (defined based on image availability) via a supervised classification of temporal (pre- and post-periods) mosaics of Landsat data. Once these layers are generated, the post-processing stage is applied in order to enhance the burned patches' shapes and eliminate salt and pepper effects. Additionally, in the case of Siberia, a burn date enhancement is applied. The general methodology flowchart illustrating the logic of the two stages is shown in Figure 2. The processing code developed in the GEE code editor platform was then translated to Python API in order to optimise and automatize the different parts of the algorithm.

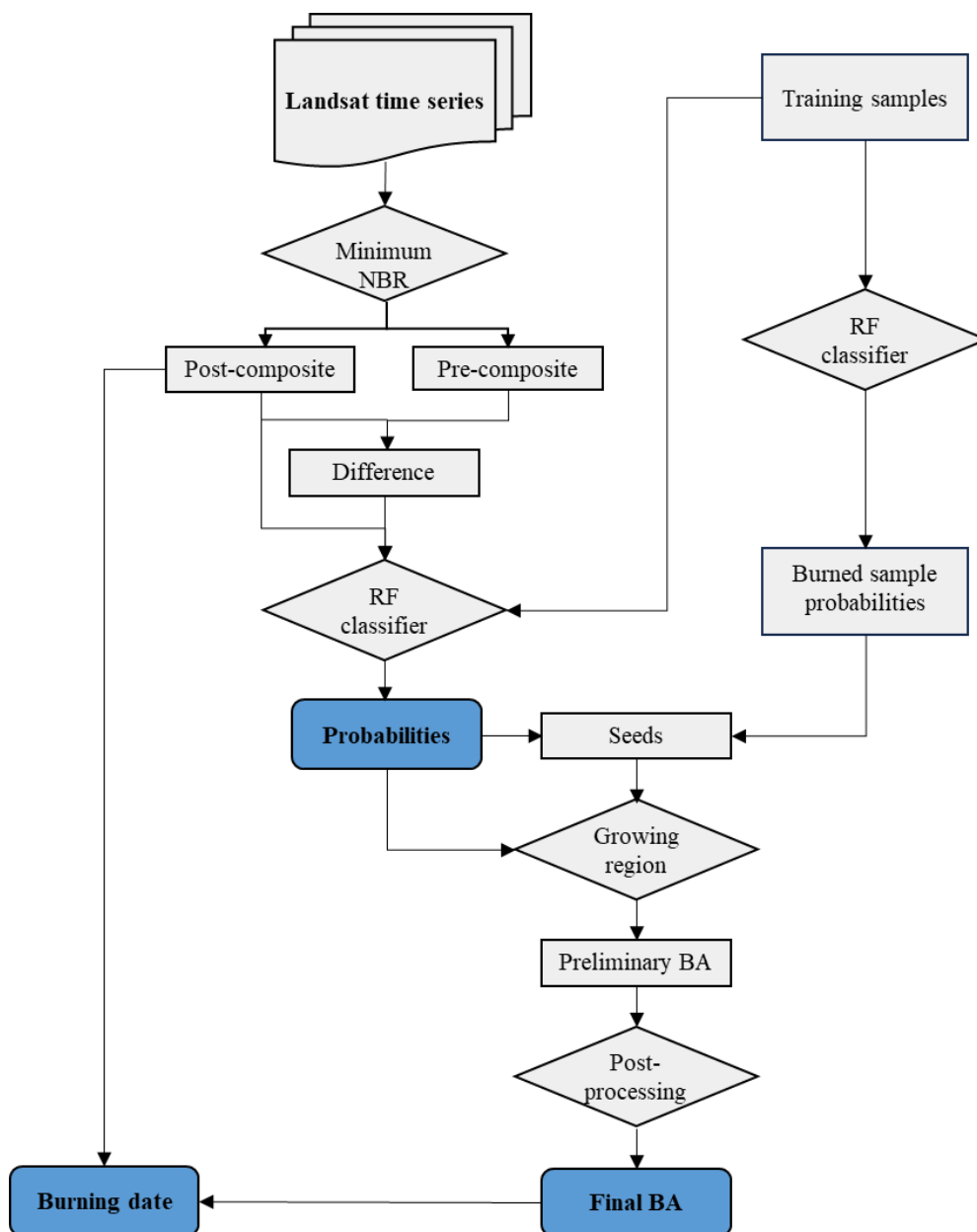


Figure 2. Flowchart of the general overview of FireCCISFDL10 BA product.

3.3.2 Selection of processing periods

In order to define the periods of processing two aspects are taken into account. The first is the number of double burns annually (pixels burning more than once at a year) on the one hand, and the availability of valid observations on the other hand. The Sahel region presents a significant risk of having double burns in a single year mainly due to the fire season that generally extends from November to March, and therefore a pixel that is burned in January and December of the same year is in fact burned in two different fire seasons. This behaviour was less observed in Amazonia as the main fire season extends from July to late October and few fires might occur outside this season (Figure 3).

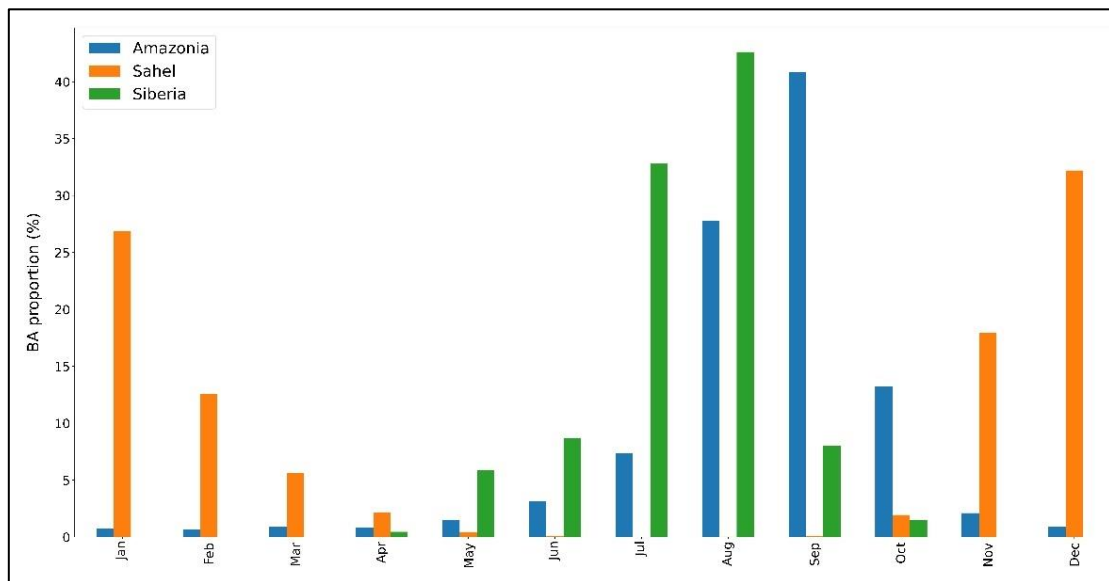


Figure 3. Fire seasonality across pilot sites using FireCCI51 time series.

Thanks to the significant availability of reliable observations in Sahel and in Amazonia even in early 2000s, a two-period compositing strategy was considered (Figure 4). The initial period spans from April to September, while the subsequent one encompasses the months from October to March. In the 90s, only Landsat-5 was effectively operating while Landsat-4 had very few acquisitions. Therefore, yearly periods were used and again the season April to March was used in order to mitigate the likelihood of missing frequent fires in Sahel. In Siberia, fires are strictly observable from March to November and the fire season spans mainly from May (i.e., overwintering fires) to September (Figure 3), and therefore a single period was processed yearly from March to November. In the case of yearly periods, the difference between dates of compositing between pre- and post-composites was also used as a predictor to capture double burns as long as the signal of burn is confident in both periods and the date difference is large (more than 6 months). The impact of the use of this variable is illustrated in Subsection 3.3.8.

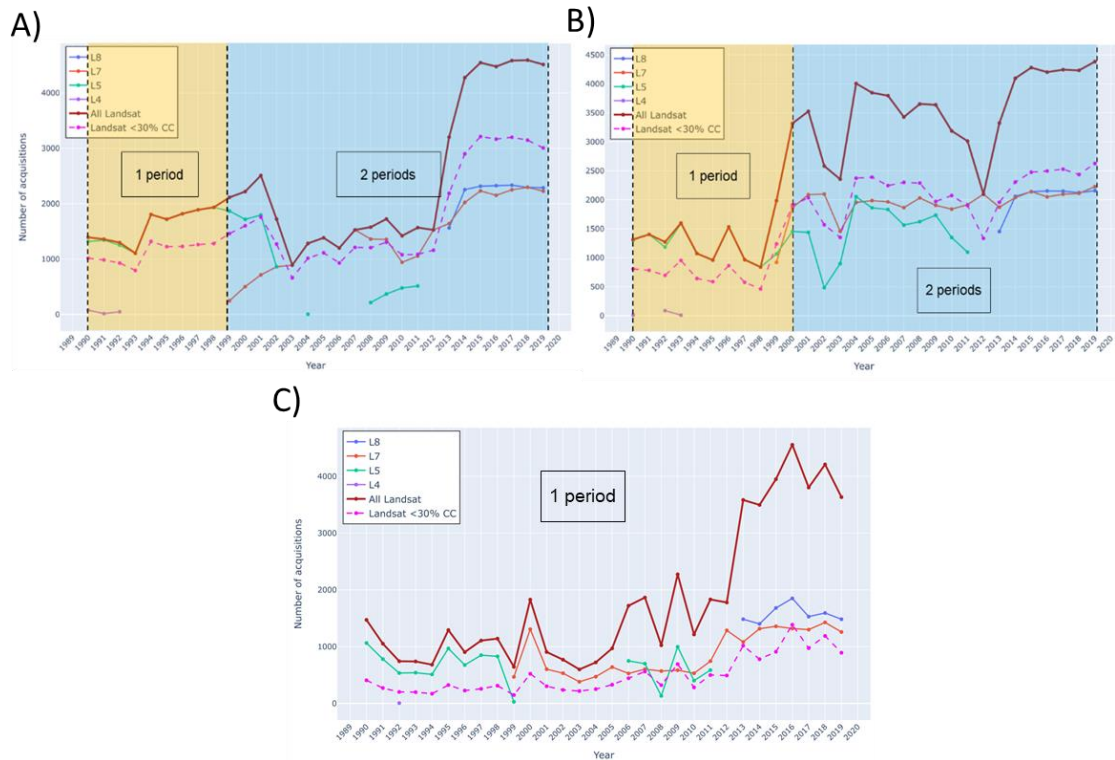


Figure 4. Number of periods proposed in each zone in function of image availability: A) Sahel; B) Amazonia; C) Siberia.

3.3.3 Spectral indices

The normalized difference between the most important spectral spaces for BA detection was added to the selected spectral bands described in

Table 1, as follows: Normalized Difference Vegetation Index (NDVI) in the Red/NIR space, Normalized Burned Ratio (NBR) in the NIR/Long SWIR and Normalized Burned Ratio 2 (NBR₂) in the Long SWIR/Short SWIR space. The equations for these indices are:

$$NDVI = \frac{\rho_{NIR} - \rho_{Red}}{\rho_{NIR} + \rho_{Red}}$$

$$NBR = \frac{\rho_{NIR} - \rho_{SWIRL}}{\rho_{NIR} + \rho_{SWIRL}}$$

$$NBR_2 = \frac{\rho_{SWIRS} - \rho_{SWIRL}}{\rho_{SWIRS} + \rho_{SWIRL}}$$

Where:

ρ_{Red} = reflectance in the Red band,

ρ_{NIR} = reflectance in the NIR band,

ρ_{SWIRS} = reflectance in the Short SWIR band and,

ρ_{SWIRL} = reflectance in the Long SWIR band.

	<p style="text-align: center;">Fire_cci Algorithm Theoretical Basis Document Small Fires Dataset Long Term</p>	Ref.:	Fire_cci_D2.2.2_ATBD_SFDL_v1.2		
		Issue	1.2	Date	18/12/2023
		Page	16		

3.3.4 Multitemporal compositing

Several studies have highlighted the importance of multitemporal compositing to enhance the burn signal. Multitemporal image composites are used to overcome problems derived from clouds, angular effects or reception issues found in image acquisitions (for instance, the Scan Line Detector (SLC) -off derived stripping effects of Landsat-7), leading to select the cleanest observation, while enhancing the burned signal (Barbosa et al., 1998; Chuvieco et al., 2005; Lizundia-Loiola et al., 2022; Sousa et al., 2003). In the case of FireCCISFDL10, we keep the minimum NBR value as an indicator of the highest signal of burn as proposed by Roteta et al. (2021a). The date of this value was used to mosaic each band in pre- and post-time series. The Julian date of burn layer of the final product was also based on this mosaicking.

3.3.5 Additional masking

Cloud mask of Landsat is based on the FMask algorithm, which usually performs well. However, in some cases it seems to miss significant cloud patches, which interfere with BA classification, especially in northern latitudes, and results in commissions or omissions (depending on whether clouds contaminate pre- or post-composites) due to the saturation of NIR and Long SWIR bands. An additional restrictive filter was applied to the aforementioned bands in order to mitigate this discrepancy. Pixels with NIR and Long SWIR values higher than 0.33 and 0.3, respectively, were filtered out of the time series to avoid cloud contamination.

Additionally, sometimes Landsat data requires additional manipulations to eliminate invalid values (e.g., due to saturation) or clouds missed by the original cloud mask. The first case was prominent in the case of Landsat-5 in 2001-2002 perhaps due to a substantial modification in the primary operating mechanism of Landsat-5 TM's scan mirror, referred to as the scan angle monitor (SAM), which caused internal synchronization issues. This malfunction resulted in diagonal patches displaying abnormal observations with exceptionally high reflectance values in the Long SWIR region and low values in Short SWIR, particularly along the edges of the scene footprint, consequently generating incorrect fire detections with high signal in the NBR2 index. To address this anomaly, the SAM system was transitioned to an alternative mode known as the bumper mode, as outlined by Storey and Choate (2004), and this adjustment successfully rectified the issue. In the pre-processing algorithm of the years 2001-2002, pixels with NBR2 lower than -0.3 were masked before compositing step (see Figure 5).

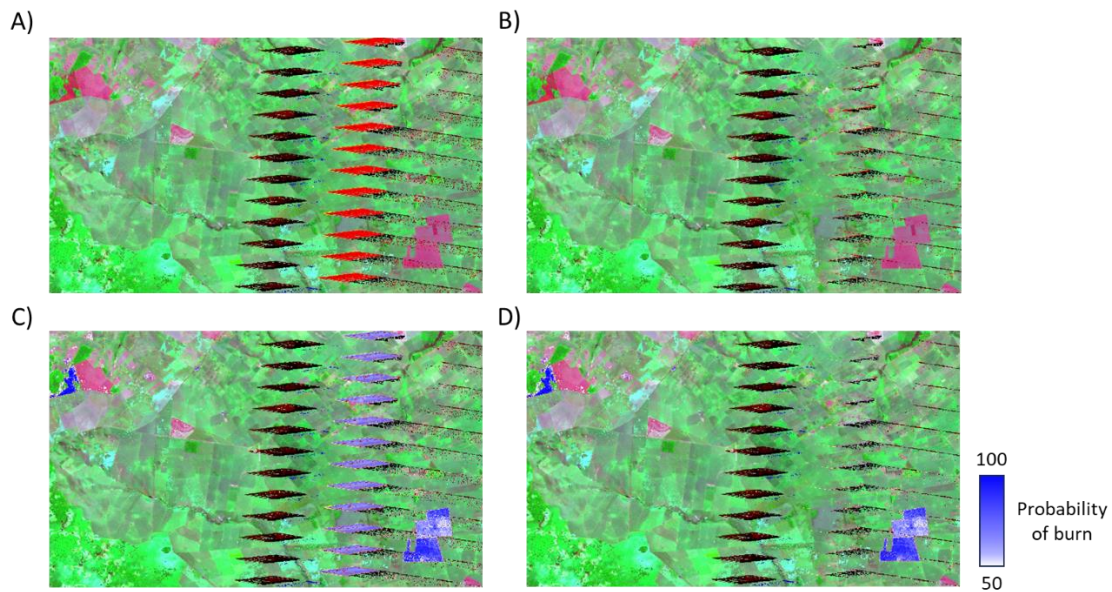


Figure 5. Mitigation of Landsat 5 defective values in 2001-2002: A) and B) are False colour composites using NBR2-NIR-Red band combination before and after applying the filter, respectively. C) and D) show the RF classification probability on top of false colour composites before and after applying the filter, respectively.

3.3.6 Random Forest Classifier

A Random Forest (RF) classifier was trained, using the burned and unburned samples the user digitized in the ‘burned’ and ‘unburned’ layers within the GEE Code Editor environment. These samples were digitized over a Long SWIR/NIR/red colour composition of the pre-fire composite, post-fire composite and pre-fire/post-fire difference visualized over the GEE map. Among other data-mining algorithms included in GEE, such as Classification and Regression Tree (CART), Naive Bayes and Support Vector Machine (SVM), RF was selected because of the fast training and prediction involved, unconstrained by the distribution of the predictor variables, reduced overfitting, robustness to outliers and non-linear data. RF classification also handles unbalanced data that are common in BA mapping. Indeed, this technique has become popular within the remote sensing community due to the accuracy of its classifications.

A Random Forest classifier is an ensemble classifier that produces multiple decision trees, using a randomly selected subset of training samples and variables. In order to balance the model accuracy alongside its complexity, RF implementation parameters were defined as:

- Number of trees: 200.
- Minimum leaf population: 10.
- Maximum nodes: 450.
- Fraction of input to bag per tree: 0.5 (default).
- Number of variables per split: square root of the number of variables (default).

All the models were trained for the year 2019 except for the case of annual models of Amazonia and Sahel, which were trained for 2004. Each model was trained using samples

	<p style="text-align: center;">Fire_cci Algorithm Theoretical Basis Document Small Fires Dataset Long Term</p>	Ref.:	Fire_cci_D2.2.2_ATBD_SFDL_v1.2		
		Issue	1.2	Date	18/12/2023
		Page	18		

collected from different variants of burn signal across the different land covers and ecoregions until the classification is optimal (confirmed through visual inspection).

3.3.7 Generation of preliminary burned area

Most of BA mapping algorithms employ a two-phased strategy. The first aims to identify most confident burned pixels called seeds (generally using active fires) to avoid omissions, then the second aims to delineate the entire burned patch using growing region methods. A similar approach was used in FireCCISFDL10, but here seeds were derived from pixels with high probability of burn rather than active fires due to the limited coverage of consistent thermal anomaly products (only from 2000 onwards). Seeds were defined as any pixel showing a probability of burn higher than the average burning probability of the burned training sample. Then, a growing process using the rook's case contiguity is applied to cover contiguous pixels with a probability higher than 50% until the entire patch is delineated. Figure 6 illustrates the process of generation of preliminary BA patches.

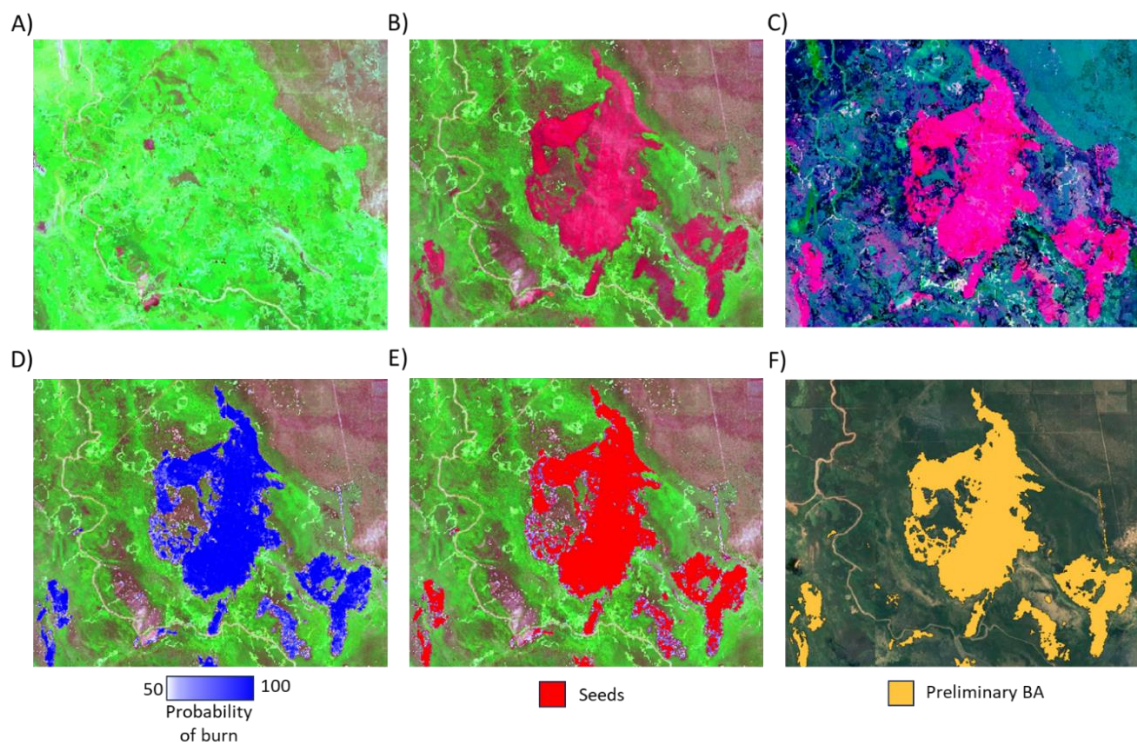


Figure 6. Burned area delineation process for some fire events in the northern border between Paraguay and Argentina for the period 2016-04-01 to 2016-09-30: A) Pre-composite (from 2015-10-01 to 2016-03-31); B) Post-composite (from 2016-04-01 to 2016-09-30); C) The difference composite; D) RF classification probability; E) Seeds; F) Delineation of preliminary BA patches. All False colour composites use NBR2-NIR-Red band combination.

3.3.8 Impact of the use of mosaicking date as predictor

In the case of yearly periods, areas affected by frequent fires that might occur in two consecutive years might be missed due to the low difference in signal between pre- and post-composites. Although this case scenario was very rare, especially with the periods

design made for Sahel and that covers the actual fire season each year, the consideration of the time between two consecutive burns was important in order to reduce the triggered omissions.

Figure 7 illustrates this enhancement, which takes into account the time difference between the two composites as a predictor for the RF model. In this way, if there is a high burn signal in the post-composite along with a sufficient time between the two composite dates to have a double burn, then the classification model captures the fire event. As a result of this operation, a significant improvement was noticed in the delineation of the burned patches. However, there were still some omissions in the patch extent, mainly in areas with a significantly high signal of burn in the pre-composite.

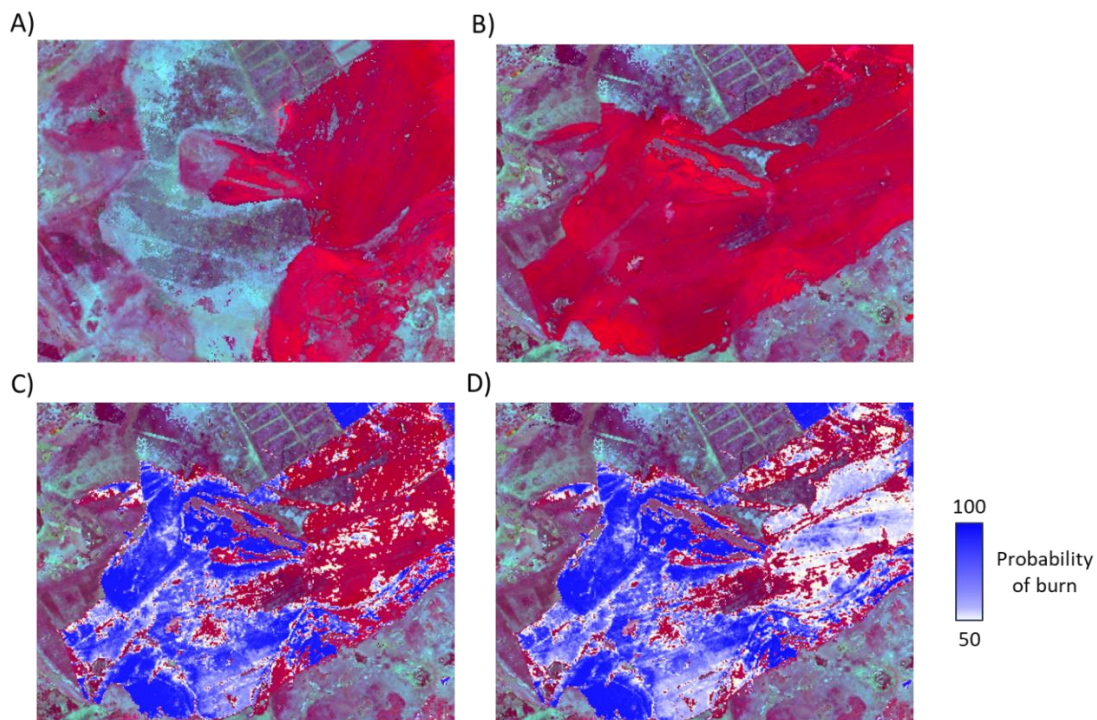


Figure 7. Impact of the use of date difference between composites in the predicted BA probability in western Siberia in 2019: A) Pre-time series false colour composite; B) Post-time series false colour composite; C) BA classification without date difference as predictor; D) BA classification including the date difference as predictor. All False colour composites use NBR2-NIR-Red band combination.

3.3.9 Generation of final burned area

In some cases, the signal within the patch is heavily heterogeneous, which leads to omission of some burned pixels with significantly low signals. In order to mitigate this discrepancy, additional growing with relaxed conditions over BA probability and the classification predictors was applied. This growing region extends for 2-km kernels around each contiguous grid cell of more than 3x3 seeds, and again the rook's case contiguity was applied (Figure 8C). This process was paramount especially in cases where patches were affected by Landsat-7 scan strips following its SLC failure occurring on May 31, 2003.

	Fire_cci	Ref.:	Fire_cci_D2.2.2_ATBD_SFDL_v1.2		
	Algorithm Theoretical Basis Document Small Fires Dataset Long Term	Issue	1.2	Date	18/12/2023
		Page	20		

This issue caused a late observation of some parts of BA patches, which led to the alteration of the signal (Figure 8B). The first unrestrictive rule was applied to probability, then a second rule took into consideration NBR2 both in post-composite and in the difference composites.

On the other hand, authors stressed that false BA detections associated with agricultural harvests could be mitigated using Red and Red edge bands (van Dijk et al., 2021). Therefore, Red and NIR bands were also considered in these rules to avoid commission errors due to harvested crops. The rules were defined as:

$$P_b \geq 40\% \quad OR \quad \{NBR2_{post} \leq 0.06 \quad AND \quad NBR2_{diff} \leq 0.005 \quad AND \\ Red_{diff} \geq 0.04 \quad AND \quad NIR_{diff} \leq -0.003\}$$

Where:

P_b is the probability of burn.

$NBR2_{post}$ and $NBR2_{diff}$ are NBR2 values for post and the difference composites, respectively.

Red_{diff} and NIR_{diff} are the Red and NIR reflectance values of the difference composite, respectively.

At this stage, 3 layers were exported from the GEE platform at grids of $2 \times 2^\circ$ below 50° parallels, $3 \times 2^\circ$ below 70° and $6 \times 2^\circ$ beyond:

- Burned area patches as ESRI shapefiles.
- The probability of burn (P_b).
- The Julian date of burn (JD).

The final phase aimed to enhance the shapes of burned patches through the elimination salt and pepper effects and the remaining empty holes within patches. This procedure was carried out using two geometrical operations; an opening followed by closing with a 3×3 kernel. Figure 8 illustrates the impact of these post-processing operations on BA patch delineation.

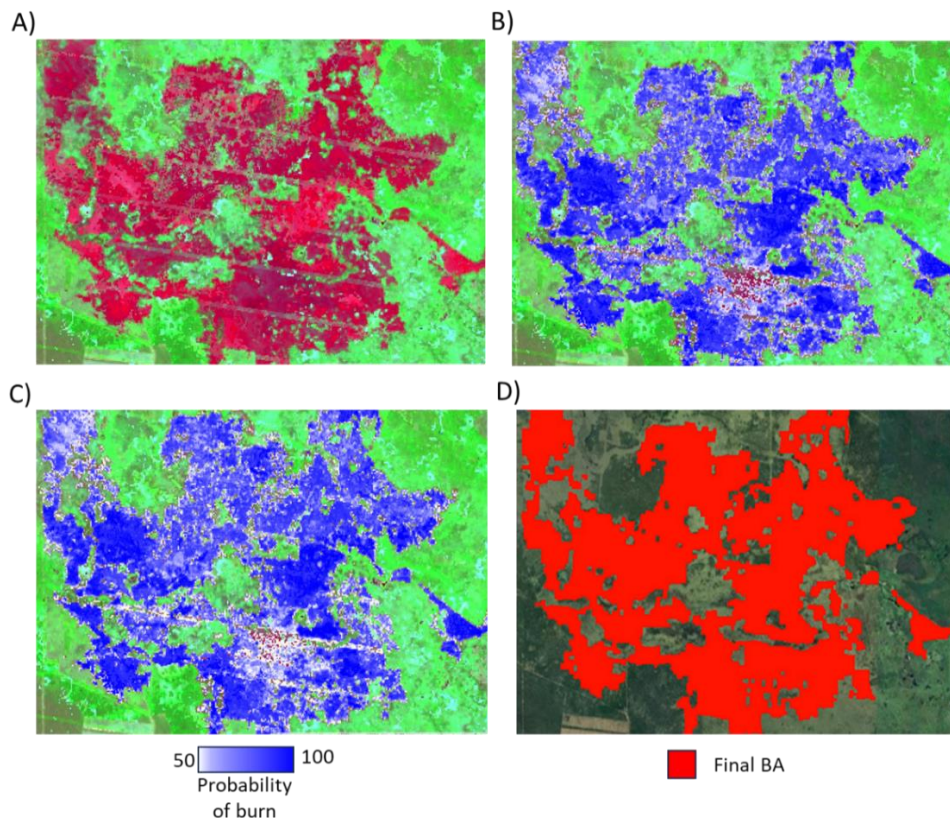


Figure 8. Generation of the final BA patches: A) Post-time series false colour composite; B) Classification probabilities of preliminary BA; C) Classification probabilities after relaxed growing region; D) Final BA patch after applying geomorphological operations.

3.3.10 Enhancement of fire detection dates in Siberia

In Siberia, the limitation in the number of valid observations was critical. Although the burn signal can last a long time in boreal forests compared to other ecosystems, the delay of time reporting made the assessment of fire regime characteristics, such as seasonality and other fire patch characteristics, inconsistent. This issue was less remarkable in Amazonia and Sahel as the number of cloud-free observations were satisfying in most cases. To overcome this problem in the Siberian region, active fire information derived from VIIRS and MODIS sensors was used to smooth fire detection dates.

For each burned pixel, if the Julian Day (JD) of burn derived from Landsat data is later than the nearest active fire date of the processing year, then it is being rectified as long as the distance is lower than 5 km, as described in Figure 9. The nearest active fire was retrieved from a Voronoi diagram.

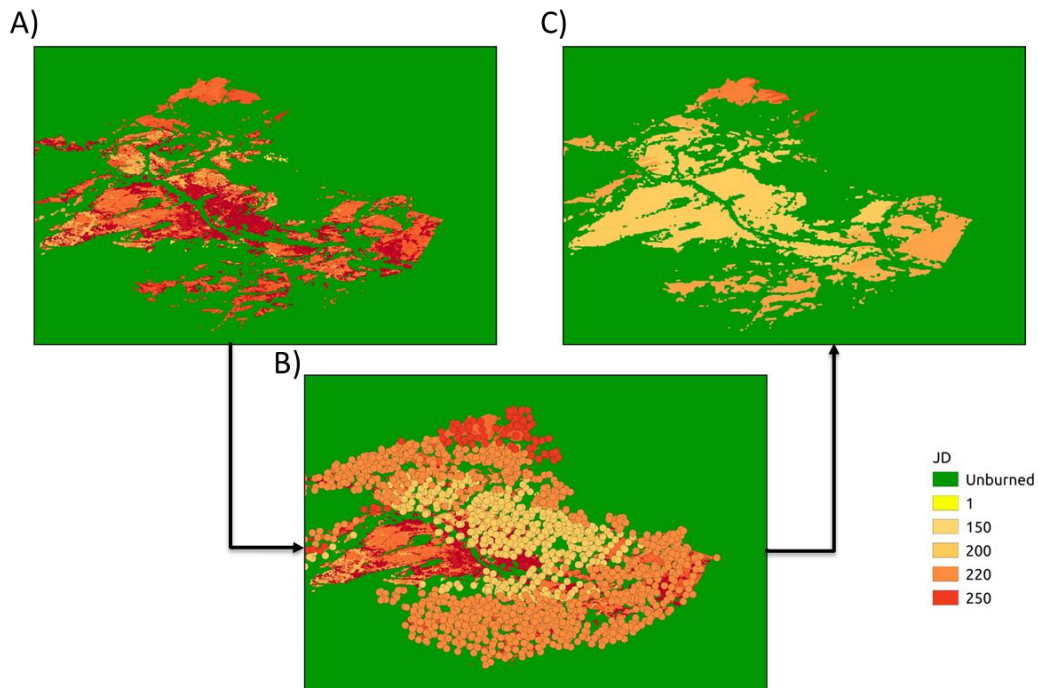


Figure 9. Correction of burn detection dates in Siberia fires using active fires: A) JD layer before date correction; B) Active fires detected within the BA patch; C) Result of the JD correction.

4 Layer output results

The outputs of FireCCISFDL10 were three monthly layers described in Table 4. All layers were geolocated using WGS84 coordinates system at 0.00025° spatial resolution (~ 30 m at the equator) and are distributed using grids of grids of $2 \times 2^\circ$ below 50° parallels, $3 \times 2^\circ$ below 70° and $6 \times 2^\circ$ beyond this latitude.

Table 4. Contents of FireCCISFDL10 layers

Layer abbreviation	Description	Possible values
JD	Julian Day of burn	<ul style="list-style-type: none"> • -2: Unburnable • -1: Unobserved • 0: Unburned • > 0: Julian day of burn
PROB	Probability of burn	<ul style="list-style-type: none"> • 0: Unburnable or unobserved • > 0: Probability of burn
LC	Land Cover of burned pixels derived from ESA CCI HRLC maps	<ul style="list-style-type: none"> • 0: Unburnable, unobserved or not burned • > 0: Land Cover of burned pixels

Figure 10 shows the output layers for a large fire observed in the border between Bolivia and Brazil in 2019 (mainly occurring between August and September) along with the post-time series composites used as a classification input.

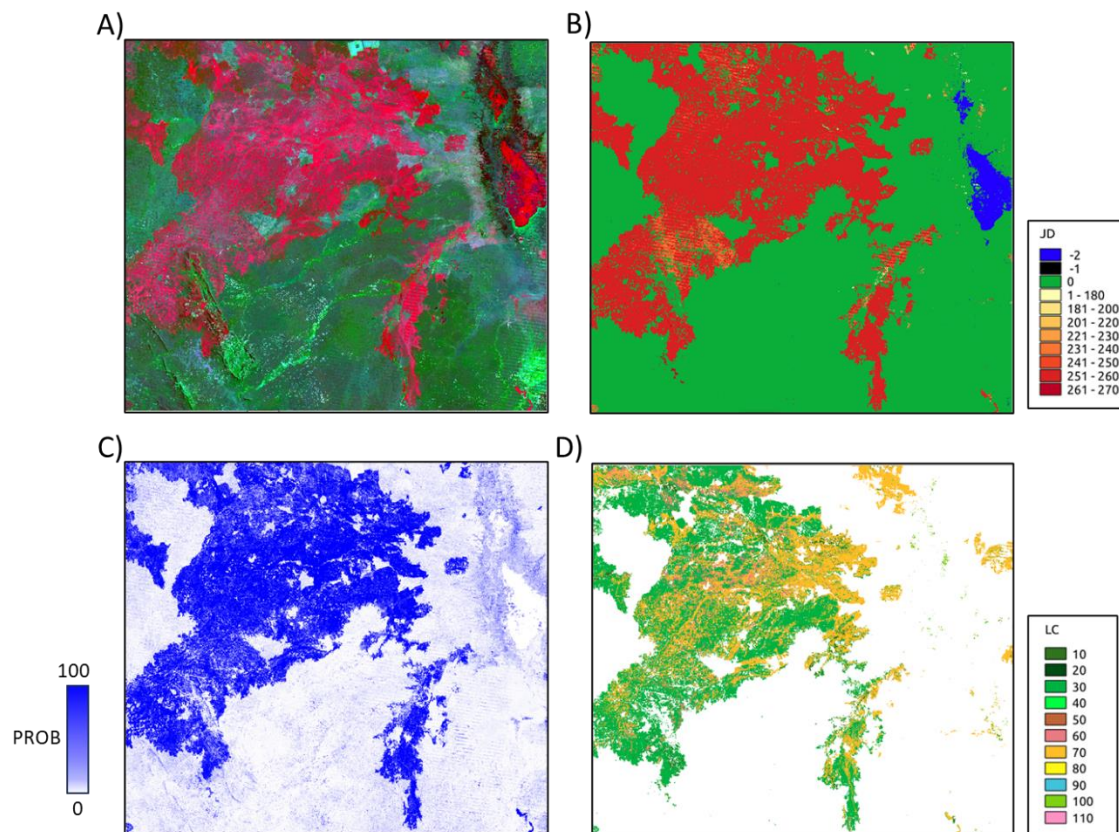


Figure 10. FireCCISFDL10 output layers' example of tile 16S060W in Amazonia for months April to September 2019 (all months combined): A) Post-time series false colour composite; B) Julian day; C) Probability; D) Land cover.

5 Limitations of the product

The FireCCISFDL10 product presents a great step towards having consistent global BA information for long-term periods at a high resolution. Nevertheless, there are some limitations that should be cautiously considered by users. Most of them have been discussed in previous sections of this document and they can be summarized as following:

1. The limited number of timely and reliable observations would be the major limitation of the product, which is due to the limited temporal accuracy of Landsat satellites especially before the Landst-8 era. In recent years, the use of combined information derived from Landsat satellites (Landsat-8 and 9) and Sentinel-2 mission (i.e., the Harmonized Landsat Sentinel product) would present a high potential to optimise the time reporting accuracy independently of active fire information and to enhance fire detection, particularly in 2012, where only Landsat-7 was operational while Landsat-5 was in decommissioning preparation. This led to significant increase of omissions in Siberia. Some efforts are ongoing to overcome this issue.
2. The Landsat-7 SLC failure occurring on May 31 2003 represents another discrepancy in the Landsat archive. Some post-processing enhancements have been performed to enhance BA patches and mitigate scan lines, which resulted in a significant improvement. However, the detection dates as well as the probability of detections were still doubtful.

	Fire_cci	Ref.:	Fire_cci_D2.2.2_ATBD_SFDL_v1.2		
	Algorithm Theoretical Basis Document Small Fires Dataset Long Term	Issue	1.2	Date	18/12/2023
		Page	24		

3. As the algorithm is independent of active fire information, areas dominated with agricultural lands might cause some confusions between actual agricultural burning and simple harvest operations. We applied some restrictive rules using Red and NIR bands to enhance the discrimination between the two case scenarios to reduce the effects of this issue.
4. Land cover information was missing in some parts of the edges of pilot sites (small strips). This information will be complemented from data sources such as the ESA LC CCI maps derived at 300-m spatial resolution.

6 References

- Alencar AAC, Arruda VLS, Silva WVd, Conciani DE, Costa DP, Crusco N, et al. (2022) Long-Term Landsat-Based Monthly Burned Area Dataset for the Brazilian Biomes Using Deep Learning. *Remote Sensing*; 14(11), 2510.
- Barbosa PM, Pereira JMC, Grégoire JM. (1998) Compositing criteria for burned area assessment using multitemporal low resolution satellite data. *Remote Sensing of Environment*; 65: 38-49.
- Bastarrika A, Alvarado M, Artano K, Martinez M, Mesanza A, Torre L, et al. (2014) BAMS: A Tool for Supervised Burned Area Mapping Using Landsat Data. *Remote Sensing*; 6: 12360-12380.
- Bastarrika A, Chuvieco E, Martín MP. (2011) Mapping burned areas from Landsat TM/ETM+ data with a two-phase algorithm: balancing omission and commission errors. *Remote Sensing of Environment*. 115, pp. 1003-1012.
- Boschetti L, Roy DP, Justice CO, Humber ML. (2015) MODIS–Landsat fusion for large area 30m burned area mapping. *Remote Sensing of Environment*; 161: 27-42.
- Boschetti, L., Roy, D. P., Giglio, L., Huang, H., Zubkova, M., & Humber, M. L. (2019). Global validation of the collection 6 MODIS burned area product. *Remote Sensing of Environment*, 235, 111490. <https://doi.org/10.1016/j.rse.2019.111490>
- Chuvieco E, Riaño D, Aguado I, Cocero D. (2002) Estimation of fuel moisture content from multitemporal analysis of Landsat Thematic Mapper reflectance data: applications in fire danger assessment. *International Journal of Remote Sensing*; 23: 2145-2162.
- Chuvieco E, Roteta E, Sali M, Stroppiana D, Boettcher M, Kirches G, et al. (2022) Building a small fire database for Sub-Saharan Africa from Sentinel-2 high-resolution images. *Sci Total Environ*; 845: 157139.
- Chuvieco E, Ventura G, Martín MP, Gomez I. (2005) Assessment of multitemporal compositing techniques of MODIS and AVHRR images for burned land mapping. *Remote Sensing of Environment*; 94: 450 – 462.
- Descals A, Gaveau DLA, Verger A, Sheil D, Naito D, Peñuelas J. (2022) Unprecedented fire activity above the Arctic Circle linked to rising temperatures. *Science*; 378: 532-537.
- ESA (2020a). Climate Change Initiative Extension (CCI+) Phase 1 New Essential Climate Variables (NEW ECVS) High Resolution Land Cover ECV

	Fire_cci	Ref.:	Fire_cci_D2.2.2_ATBD_SFDL_v1.2		
	Algorithm Theoretical Basis Document Small Fires Dataset Long Term	Issue	1.2	Date	18/12/2023
		Page	25		

(HR_LandCover_cci) Product User Guide (PUG).
https://climate.esa.int/media/documents/CCI_HRLC_Ph1-D1.1_URD_v2.0.pdf.

ESA (2020b). Climate Change Initiative Extension (CCI+) Phase 1 New Essential Climate Variables (NEW ECVs) High Resolution Land Cover ECV (HR_LandCover_cci) User Requirement Document (URD).
https://climate.esa.int/media/documents/CCI_HRLC_Ph1-D1.1_URD_v2.0.pdf.

Franquesa, M., Lizundia-Loiola, J., Stehman, S. V., & Chuvieco, E. (2022). Using long temporal reference units to assess the spatial accuracy of global satellite-derived burned area products. *Remote Sensing of Environment*, 269, 112823.
<https://doi.org/10.1016/j.rse.2021.112823>

GCOS (2022). The 2022 GCOS ECVs Requirements. (GCOS-245). Geneva, Switzerland: World Meteorological Organization.

Hantemirov RM, Corona C, Guillet S, Shiyatov SG, Stoffel M, Osborn TJ, et al. (2022) Current Siberian heating is unprecedented during the past seven millennia. *Nature Communications*; 13, 4968.

Lizundia-Loiola J, Franquesa M, Khairoun A, Chuvieco E. (2022) Global burned area mapping from Sentinel-3 Synergy and VIIRS active fires. *Remote Sensing of Environment*; 282, 113298.

Long, T.; Zhang, Z.; He, G.; Jiao, W.; Tang, C.; Wu, B.; Zhang, X.; Wang, G.; Yin, R. (201) 30 m Resolution Global Annual Burned Area Mapping Based on Landsat Images and Google Earth Engine. *Remote Sens.* 9, 11, 489.

Ramo R, Roteta E, Bistinas I, van Wees D, Bastarrika A, Chuvieco E, et al. (2021) African burned area and fire carbon emissions are strongly impacted by small fires undetected by coarse resolution satellite data. *Proceedings of the National Academy of Sciences*; 118: e2011160118.

Randerson JT, Chen Y, Werf GR, Rogers BM, Morton DC (2012). Global burned area and biomass burning emissions from small fires. *Journal of Geophysical Research: Biogeosciences*; 117 - G040: 1-23.

Roteta E, Bastarrika A, Franquesa M, Chuvieco E. (2021a) Landsat and Sentinel-2 Based Burned Area Mapping Tools in Google Earth Engine. *Remote Sensing*; 13(4), 816.

Roteta E, Bastarrika A, Ibisate A, Chuvieco E. (2021b) A preliminary global automatic burned-area algorithm at medium resolution in Google Earth Engine. *Remote Sensing*; 13(21), 4298.

Roteta E., Bastarrika A., Padilla M., Storm T., Chuvieco E. (2019) Development of a Sentinel-2 burned area algorithm: Generation of a small fire database for sub-Saharan Africa, *Remote Sens. Environ.*, 222 1-17.

Roy D, Landmann T. (2005) Characterizing the surface heterogeneity of fire effects using multi-temporal reflective wavelength data. *International Journal of Remote Sensing*; 26: 4197-4218.

Scholten RC, Coumou D, Luo F, Veraverbeke S. (2022) Early snowmelt and polar jet dynamics co-influence recent extreme Siberian fire seasons. *Science*; 378: 1005-1009.

	<p style="text-align: center;">Fire_cci Algorithm Theoretical Basis Document Small Fires Dataset Long Term</p>	Ref.:	Fire_cci_D2.2.2_ATBD_SFDL_v1.2			
		Issue	1.2	Date	18/12/2023	
		Page				26

- Sousa AMO, Pereira JMC, Silva JMN. (2003) Evaluating the performance of multitemporal image compositing algorithms for burned area analysis. *International Journal of Remote Sensing*; 24: 1219–1236.
- Storey JC, Choate MJ. (2004) Landsat-5 bumper-mode geometric correction. *IEEE Transactions on Geoscience and Remote Sensing*; 42: 2695-2703.
- Stroppiana D, Sali M, Busetto L, Boschetti M, Ronghetti L, Franquesa M, et al. (2022) Sentinel-2 sampling design and reference fire perimeters to assess accuracy of Burned Area products over Sub-Saharan Africa for the year 2019. *ISPRS Journal of Photogrammetry and Remote Sensing*; 191: 223-234.
- van Dijk D, Shoaie S, van Leeuwen T, Veraverbeke S. (2021) Spectral signature analysis of false positive burned area detection from agricultural harvests using Sentinel-2 data. *International Journal of Applied Earth Observation and Geoinformation*; 97, 102296.
- Wei M, Zhang Z, Long T, He G, Wang G. (2021) Monitoring Landsat Based Burned Area as an Indicator of Sustainable Development Goals. *Earth's Future*; 9, e2020EF001960.
- Zheng B, Ciais P, Chevallier F, Yang H, Canadell JG, Chen Y, et al. (2023) Record-high CO₂ emissions from boreal fires in 2021. *Science*; 379: 912-917.

Annex: Acronyms and abbreviations

API	Application Programming Interface
ATBD	Algorithm Theoretical Basis Document
BA	Burned Area
BAMT	Burned Area Mapping Tools
CART	Classification And Regression Tree
CCI	Climate Change Initiative
CE	Commission Error
ECV	Essential Climate Variables
ENSO	El Niño-Southern Oscillation
ESA	European Space Agency
ESRI	Environmental Systems Research Institute
ETM+	Enhanced Thematic Mapper Plus
FIRMS	Fire Information for Resource Management System
FMask	Function of Mask
GCOS	Global Climate Observing System
GEE	Google Earth Engine
HRLC	High-Resolution Land Cover
JD	Julian Day
LaSRC	Land Surface Reflectance Code
LC	Land Cover
LEDAPS	Landsat Ecosystem Disturbance Adaptive Processing System
MODIS	Moderate Resolution Imaging Spectroradiometer
NASA	The National Aeronautics and Space Administration
NBR	Normalized Burned Ratio
NBR2	Normalized Burned Ratio 2
NDVI	Normalized Difference Vegetation Index
NIR	Near InfraRed
NPP	National Polar-orbiting Partnership
OE	Omission Error
OLI	Operational Land Imager
PROB	Probability of burn
QA	Quality assessment
RF	Random Forest
SAM	Scan Angle Monitor
SFD	Small Fire Dataset
SLC	Scan Line Corrector
SR	Surface Reflectance
SVM	Support Vector Machine
SWIR	Short Wave Infra-Red
TM	Thematic Mapper
USGS	United States Geological Survey
VIIRS	Visible Infrared Imaging Radiometer Suite
WGS	World Geodetic System